Construction and Building Materials 230 (2020) 116928

Contents lists available at ScienceDirect

Construction and Building Materials

journal homepage: www.elsevier.com/locate/conbuildmat

Influence of fine cement sand paste in preparation of cementitious materials

Wajahat Sammer Ansari, Jun Chang *

School of Civil Engineering, Dalian University of Technology, Dalian 116024, Liaoning, China

HIGHLIGHTS

- A new method for mortar preparation of fine cement was proposed.
- Fine cement effect on cement composites are analyzed.
- Porosity was demonstrated by MIP and image J software.
- Crack widths in ITZ were evaluated.

GRAPHICAL ABSTRACT

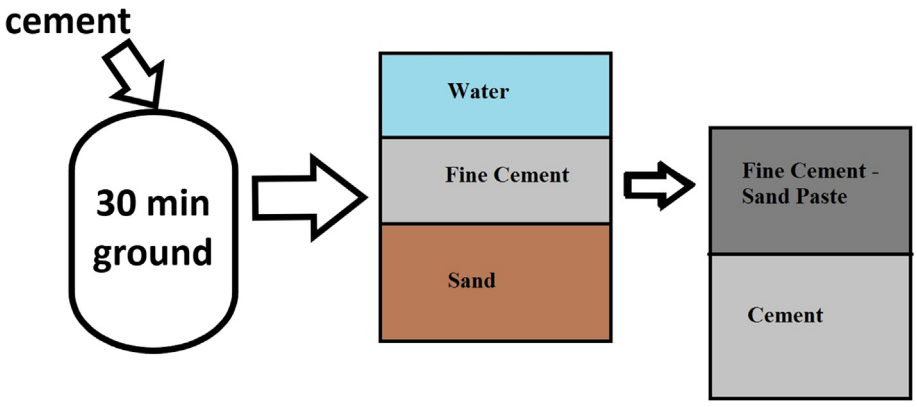

ARTICLE INFO

Article history:
Received 7 June 2019
Received in revised form 5 August 2019
Accepted 8 September 2019
Available online 20 September 2019

Keywords:
Interfacial transition zone
Fine cement
Sulfoaluminate cement
Image J
Hydration products
Mortar
Fine cement
MIP
SEM
TGA

ABSTRACT

The fine cement replacement in conventional cement plays an important role in the microstructure development. To date, no studies have been done to analyze the mixing of fine cement, sand, and water under partial replacement of conventional cement. Therefore, this paper explores the influence of fine cement sand paste on cementitious materials. In this study, the fine calcium sulfoaluminate cement (CSA) cement was prepared to have an average diameter of 2.4 μm. Furthermore, its partial replacement at different percentages was investigated and compared to the ordinary Portland cement (OPC) system. For mortar preparation, a new method is proposed in this paper. First of all, the fine cement, sand, and water are mixed to form a paste and then conventional cement is added. Results emphasized that strength, porosity, permeability, and crack widths in the interfacial transition zone (ITZ) are more affected by this technique. It is concluded that partial replacement of 20% fine CSA content results in improved strength by 30%–35% as compared to the OPC system. Moreover, porosity and permeability were also reduced by 60%–70%. Also, the crack widths at the interfacial transition zone (ITZ) were also reduced up to 60%. This new technique for mortar preparation of fine cement can be applied to form a good microstructure network in cementitious composites.

© 2019 Elsevier Ltd. All rights reserved.

1. Introduction

Fine ordinary Portland Cement (OPC) exhibits high early heat of hydrations and contributes to a good strength development in cementitious composites [1]. The replacement of OPC cement by

* Corresponding author.
E-mail address: mlchang@163.com (J. Chang).

https://doi.org/10.1016/j.conbuildmat.2019.116928
0950-0618/© 2019 Elsevier Ltd. All rights reserved.

materials such as silica fume, slag, carbon Nano-tubes, ceramic waste, and fine kaolinite sand at optimum content resulted in improved microstructural and strength properties [2–4]. It is reported that by replacement of 20% fine ground OPC in conventional OPC resulted in increased strength, decreased porosity, and improvement of the interfacial transition zone (ITZ) as compared to that of conventional OPC system [5]. Previous studies showed that by deploying fine materials as a replacement in cementitious composites exhibit good energy absorption capacities [6–8]. Past research shows that it's difficult to store and develop fine OPC as it exhibits high carbon dioxide emissions which are not environment-friendly [9]. Another problem is the requirement of grinding agents at optimum values to have good fine cement [10].

Also, few studies had been done to reduce carbon emissions in the cement industry [11]. The calcium sulfoaluminate cement (CSA) is considered environment-friendly materials since their manufacturing process releases less carbon dioxide emissions into the atmosphere than that of OPC [12]. The strength development of CSA is also relatively higher than OPC cement at early ages [13]. CSA cement needs less firing temperatures about 1230–1350 °C, and during calcination, it gives lower calcium oxide contents which result in less carbon dioxide emissions [14]. CSA cement after 28 days of curing exhibits good porosity behavior as compared to that of conventional OPC [15]. Tan et al. [16] reported good porosity, high compressive strength, hydration products, and different phases of structures at the early stage of CSA with the replacement of nanomaterials. Kontoleontos et al. [17] concluded that by using nanomaterials in cement composites exhibited good porosity behavior and thus presented a structure having high densities. Zhang et al [18] analyzed the effects of fine CSA cement by using scanning electron microscope (SEM), X-ray powder diffraction (XRD), thermo gravimetric analysis (TGA) by deploying different grouting materials. They concluded that ettringite and gibbsite (AH_3) are main indicators to contribute strength. Influence of fine materials in cement also had a special effect on the ITZ; whereas ITZ is defined as a wall effect [19] between the aggregate and cement paste in a cementitious composite having a porous structure. The ITZ between cement and aggregate particles is shown in Fig. 1 [20]. This wall effect should be minimized in a manner resulting in fewer pores, high strength, and thus contributes to effective microstructure.

Many methods have been employed previously to analyze the ITZ [21,22]. According to Kumar Mehta's [23] research, it was concluded that during OPC hydration CH and C-S-H start filling the pore spaces and so exhibits to make non-porous structure [24] and thus increased the strength of ITZ. In SEM, the location of ITZ can be analyzed. For SEM, the sampling should be done so, that the structure represents the true nature of samples [25]. In the OPC system, the ITZ can be analyzed by the Ca/Si ratio because it consists of C-S-H gel and CH hydrates [26]. For C-S-H its value is less and for the presence of CH, its ratio goes above 10. The C-S-H is directly related to strength and stiffness, therefore, Ca/Si ratio should be less for OPC systems [27]. Carrara and De Lorenzis [28] investigated during their modal studies based on ITZ's of different cement samples that the ITZ thickness is equal to 1.5–2.0 times of the mean particle diameter of cement clinker.

The cementitious efficiency can be increased at an early stage by maintaining the optimum content of fine cement [29]. If the carbon dioxide emission can be controlled and fine cement can be prepared in a short time that will be an economical and environmentally friendly decision [30]. According to the characteristics and behavior of fine cement, as stated in previous research, it may be able to prepare a fine cement mortar with excellent performance. Thus, a fine CSA cement is prepared and a new method for mixing fine cement in mortar has been introduced in this paper. The objective of mortar preparation is to cover the cement particles from fine cement particles as illustrated in Fig. 1. At present this kind of aspect has not been introduced extensively while no research till now focuses on preparation of mortar by fine cement. Therefore, this study focuses on influence of fine cement sand paste and their effects on mechanical properties, early age hydration, and microstructure properties. TGA and SEM are used to research the hydration products while, MIP and image J analysis are used to research porosity and permeability. In addition, crack widths in ITZ are also identified by image J software. In future, this study will work as a guidance on application and preparation of fine cement in cementitious composites.

2. Materials and methods

2.1. Characteristics of raw material

2.1.1. Cement

Two types of cement are used in this study. The first type is ordinary Portland cement (OPC) and the other is calcium sulfoaluminate cement (CSA). The chemical composition of cement by using XRF are shown in Table 1. Physical and chemical properties are enlisted in Table 2. Densities are calculated by true density meter by JWGB Beijing Co. Ltd.

Fig. 2 represents the CSA and OPC gradation curve. The different particle sizes distributions [31] are shown in Table 3. Which are calculated with the help of Malvern master sizer 2000 machine

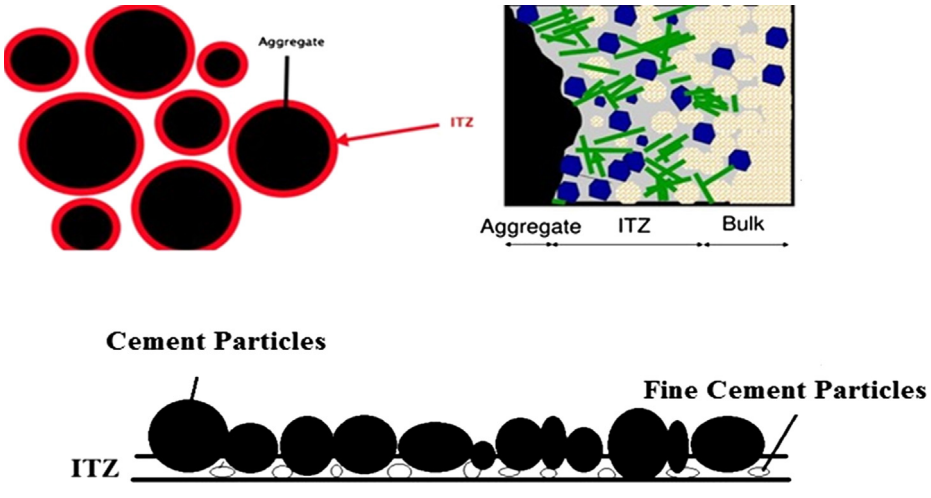

Fig. 1. ITZ between cement paste and aggregate.

Table 1
Chemical composition of the OPC and CSA.

	CaO	Fe_2O_3	SiO_2	MgO	Al_2O_3	K_2O	SO_3	Na_2O	Loss
OPC	61.13	2.89	22.65	3.75	5.44	0.81	2.5	0.77	2.37
CSA	40.5	2.6	8.5	2.5	36	0.3	9.1	0.1	0.4

Table 2
Properties of cement.

	Setting time (min)		Compressive strength (MPa)			Flexural strength (MPa)			Density (kg/m^3)
	Initial	final	1d	3d	28d	1d	3d	28d	
OPC	>45	<600	14	20	48.9	2	4.2	6.7	3126.56
CSA	12–30	20–50	30	42.5	56.6	6.0	6.5	7.2	2934.24

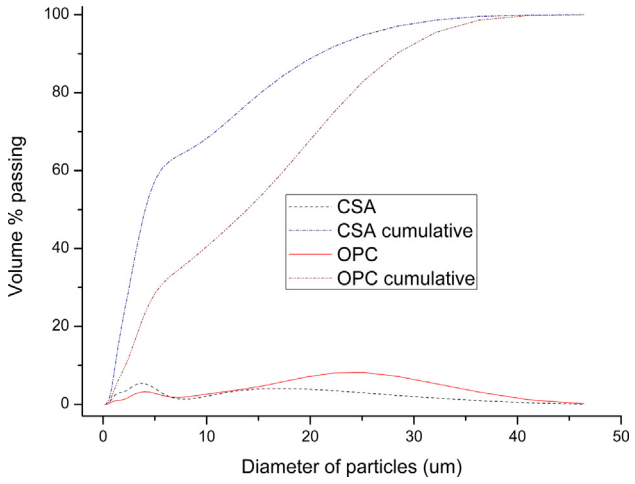

Fig. 2. % passing of OPC and CSA cement.

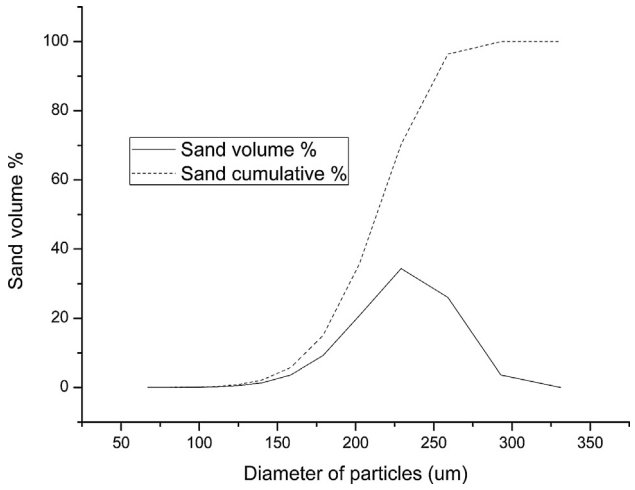

Fig. 3. Sand gradation curves.

according to ASTM E2651-10 [32]. In Table 3 D50 is the size in microns at which 50% of the sample is smaller and 50% is larger. D10, D90, and D95 is the size of the particles below which 10, 90, 95% of the sample lies. While D [4, 3] is the volume-weighted mean or mass moment mean diameter. It can be concluded here that the mean diameter of OPC is 1.65 times than CSA.

2.1.2. Sand

The sand used in our research is China ISO standard sand according to ISO679 & EN196-1 specifications manufactured by Xiamen ISO Standard Sand Co., Ltd. Sand is natural and siliceous sand having rounded particles and having siliceous contents more than 98% in it. The true density of sand by true density meter is 2667.58 kg/m^3. The gradation curve for sand is shown in Fig. 3. The particle distribution of sand is shown in Table 3.

2.1.3. Fine CSA

Calcium sulfoaluminate cement (CSA) was ground in a planetary ball mill (Retsch Co., Germany; Model No.: PM 100) for 30 min, 1 h and 2 h. The weight of balls in the grinding mill was 1 kg. The mill was operated at 400 rpm. The percentage volume and cumulative volume percentage of different ground cement are shown in Fig. 4.

From Fig. 4, it is seen that the cement at 2 h is less in particle size than others; but the cumulative graph of 30 min, 1 h, and 2 h shows very little deviations. So, due to the economic point of view, the 30 min ground time is selected in this study; as there is less deviation between the particle size of 30 min, 1 h, and 2 h. In Table 3, it is clearly shown that the median diameter of 30 min, 1 h and 2 h grinding time is almost equal. So, it's appropriate to take 30 min grinding time for our research.

Table 3
Particle size distributions (um).

	D10	D50	D90	D95	D97	D[4,3]
OPC	2.2	13.9	28.3	31.7	33.7	14.35
CSA	1.2	4.6	23.5	28.7	31.5	8.7
Ground CSA (30 min)	0.9	2.3	4.3	4.9	5.2	2.4
Ground CSA (1 h)	0.82	2.10	4.22	4.80	5.16	2.33
Ground CSA (2 h)	0.79	1.98	4.09	4.62	4.93	2.23
Sand	169.9	213.9	247.7	255.8	260.8	210.9

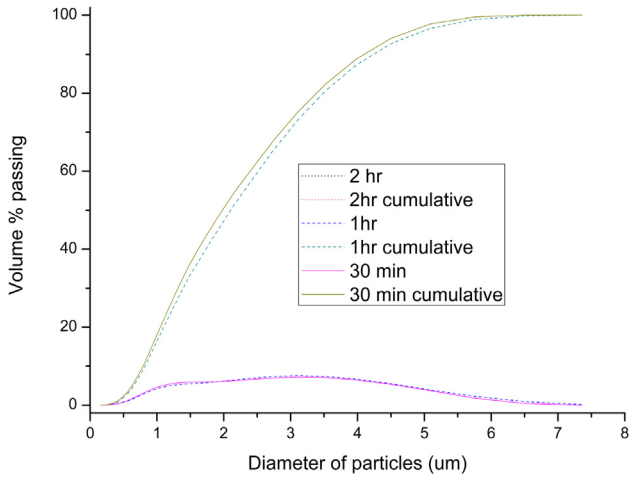

Fig. 4. Ground cement gradation curves.

2.2. Methods

2.2.1. Fluidity

Fluidity is checked according to ASTM C1437—15 [33] to find the appropriate water-cement ratio for mortar preparation. The cement-sand ratio was taken to be 1:3. The fluidity is maintained at 180–220 mm to form a dense mixture and good workability [34,35].

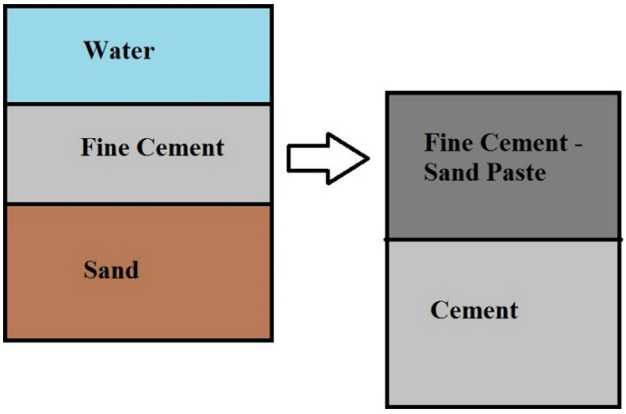

Fig. 5. Mixing process of mortar.

2.2.2. Strength

The flexural and compressive strengths and their energy absorption capacities were analyzed. According to ASTM C348-02 [36] & C349 – 18 [37] at 1, 3 and 28 days, respectively. For the mortar preparation, the partial percentages of fine cement are mixed together firstly with sand; and then water was added to form a paste and lastly, the conventional cement is added as shown in Fig. 5.

2.2.3. Hydration heat

The fine cement at different partial percentages in conventional cement was prepared and their effect was checked by micro-calorimeter for 72 h in accordance with ASTM C 1702 [38]. Also, OPC, CSA, and fine CSA were also investigated.

2.2.4. Thermogravimetric analysis

Thermogravimetric analysis (TGA) was done for cement pastes after 3 days of hydration as in accordance with ASTM E1142-15 [39]. Different hydration products after 3 days of hydration were analyzed by Mettler-Toledo (TG/DSC1; 10 ± 1 mg dry, ground pastes were tested from 35 °C to 1000 °C at a heating rate of 10 °C/min, and nitrogen was used as a protective gas).

2.2.5. MIP

Mercury Intrusion Porosimetry (MIP) analysis of mortar samples after being cured at 28 days was observed by MIP Auto Pore, America Apparatus in accordance with ASTM D4404 [40].

2.2.6. SEM

SEM analysis was done to analyze the microstructure. Image J analysis was done to find the crack widths in the interfacial transition zone (ITZ) region [41–43] and to study the porosity analysis of different samples from their SEM pictures [44,45]. The method for porosity analysis by Image J is described in Fig. 6.

3. Results and analysis

3.1. Fluidity

Fluidity test was analyzed at different water-cement ratios. The results can be seen in Fig. 7 fluidity test for OPC and CSA in which water-cement ratio and flow in millimeters have been shown. Different water-cement ratios have been selected to check fluidity rates.

Winnefald and Lottenbach concluded that CSA cement requires more water for hydration than OPC [46]. It is focused that the

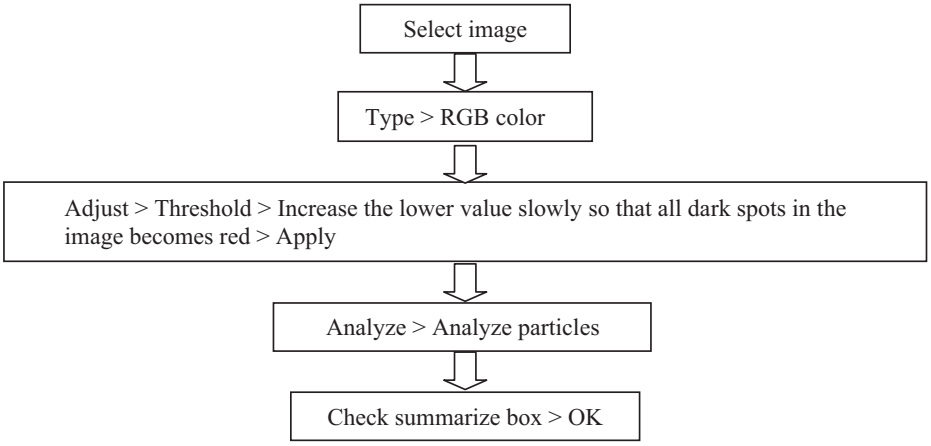

Fig. 6. Method for porosity analysis by Image J.

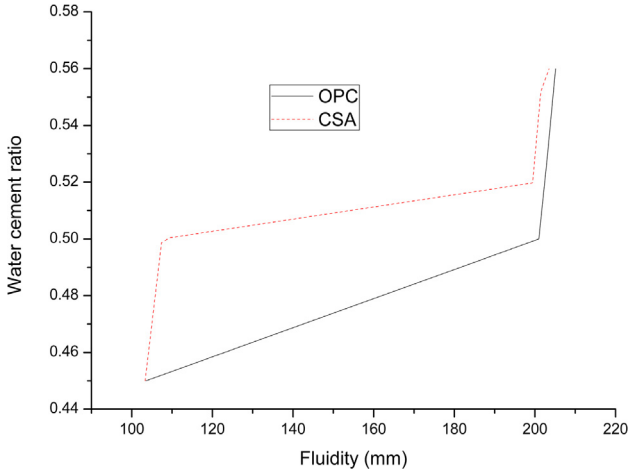

Fig. 7. Fluidity test for OPC and CSA.

fluidity rates for both OPC and CSA with a water-cement ratio of 0.5 and 0.55, respectively are similar. Therefore in our study, we will apply OPC water-cement ratio at 0.5 and CSA water-cement ratio at 0.55. By using regression analysis we discovered the cubic relation between OPC cement and its fluidity rate at a 95% confidence interval. The regression Eq. (1) found to be R^2 = 99.9% which predicts an excellent modal [47,48]

$$X = -30851 + 175962Y - 332172Y^2 + 208909Y^3 \quad (1)$$

While CSA and its fluidity show cubic model with R^2 = 96% which exhibits a good model. The correlation is shown in Eq. (2)

$$Y = -7.020 + 0.1549Z - 0.001028Z^2 + 0.000002Z^3 \quad (2)$$

where,

X = Fluidity of OPC Cement
Y = Water-Cement Ratio
Z = Fluidity of CSA Cement

Finally, we also calculated the relation between OPC and CSA fluidity at constant water-cement ratios. The correlation factor shows R^2 = 100.0% which exhibits an excellent model and is shown in Eq. (3). Where X and Z are defined as above

$$X = -10381 + 203.8Z - 1.243Z^2 + 0.002442Z^3 \quad (3)$$

3.2. Impact of fine cement sand paste on strength

Flexural and compressive strength tests had been carried out for the OPC sample at 0.5 water-cement ratio and CSA samples at 0.55 water-cement ratio. The CSA samples having 0, 10, 20, 30% of fine CSA replacement in conventional CSA was found. Cement sand ratio is maintained at 1:3. Flexural energy absorption capacities are defined as the total area under the load-deflection curve [49]. Which is shown in Table 4. The CSA 10%, CSA 20% CSA 30% explains having 10, 20, 30% replacement of fine CSA. It is noted that OPC has less strength and capacity than CSA.

The correlation between flexural strength and partial percentages from 0 to 30% of fine CSA is investigated. Results conclude quadratic regression modal for 1 d, 3 d and 28 d of curing. The R^2 for correlations are 98%, 90%, and 98% at 95% confidence interval concluding an excellent model. The models are shown in Eqs. (4) (5) and (6).

$$a_1 = 5.970 + 0.1320b - 0.003000b^2 \quad (4)$$

$$a_3 = 6.400 + 0.1900b - 0.005000b^2 \quad (5)$$

$$a_{28} = 7.535 + 0.1635b - 0.004750b^2 \quad (6)$$

where,

a_1 = 1 day flexural strength of CSA mortar
a_3 = 3 day flexural strength of CSA mortar
a_{28} = 28 day flexural strength of CSA mortar
b = Replacement of ground CSA in %

The compressive strength results has been shown in Table 5. It is focused that 20% replacement of fine cement gives good compressive strength as compared to others. It also shows good compressive energy absorption capacities.

The correlation between compressive strength and replacement of fine CSA from 0% to 30% is investigated. The regression models show R^2 as 99.7%, 91%, and 90% respectively concluding an excellent model. The models are shown in equation which shows a relationship between compressive strengths of cement mortar at 1, 3 and 28 days and replacement percentage by fine cement from 0 to 30% (7) (8) & (9).

$$c_1 = 37.18 + 0.1035b - 0.001750b^2 \quad (7)$$

$$c_3 = 52.02 + 0.5025b - 0.00625b^2 \quad (8)$$

$$c_{28} = 57.44 + 0.4495b - 0.008750b^2 \quad (9)$$

where

c_1 = 1 day compressive strength of CSA mortar
c_3 = 3 day compressive strength of CSA mortar
c_{28} = 28 day compressive strength of CSA mortar

3.3. Isothermal calorimetry

Hydration heat curves for OPC, CSA, and fine CSA are analyzed (water-cement ratio for OPC as 0.5 and for CSA samples as 0.55) which is shown in Fig. 8. CSA and fine CSA peak show at 2 h with a shoulder after 3 h. The OPC peaks at 12.5 h with a shoulder after

Table 4
Flexural strength (MPa) and its energy absorption capacities.

	Flexural strength (MPa)			Flexural energy absorption capacity (Joules)		
	1d	3d	28d	1d	3d	28d
OPC	3.6	6.1	6.8	0.15	0.78	0.77
CSA	6.1	6.5	7.5	0.57	0.86	0.77
CSA 10%	6.9	7.5	8.8	0.72	0.97	1.04
CSA 20%	7.5	8.5	8.8	0.81	1.79	1.18
CSA 30%	7.2	7.5	8.2	0.92	0.97	0.66

Table 5
Compressive strength (MPa) and its energy absorption capacities.

	Compressive strength (MPa)			Compressive energy absorption capacity (Joules)		
	1d	3d	28d	1d	3d	28d
OPC	16	26	48	39	46	77.5
CSA	37.2	52.5	57.8	76	81	92.8
CSA 10%	38	55	60	77	77	106
CSA 20%	38.6	61	64	78	79	106
CSA 30%	38.7	61	62.7	75	88	84.7

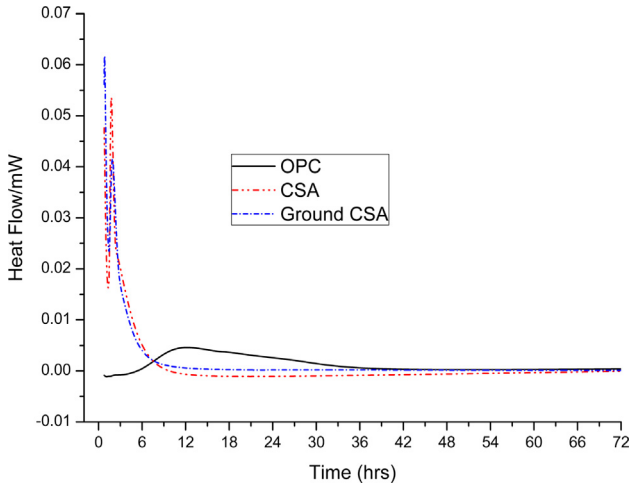

Fig. 8. Hydration heat curves.

37 h. These results conclude that formation of C-S-H in OPC is relatively slow then CSA. By noticing the height of peaks an OPC has a high peak at 0.0046 while, CSA and fine CSA are at 0.05 and 0.06. Therefore CSA early strength development is relatively fast as compared to OPC. While the total heat of hydration is 64.48617, 77.9042 and 88.0257 J per gram for OPC, CSA and fine CSA respectively.

Also, we investigated the behaviors with fine CSA partial replacement at 10, 20 and 30% in CSA pastes and their heat of hydrations are 80.73612, 82.63986 and 86.7538 J per gram.

3.4. Thermogravimetric analysis

OPC and CSA samples were tested and analyzed by thermogravimetric analysis (TGA). DTG curves having good clarity is shown in Fig. 9. Stats from TGA are shown in Table 6.

According to ASTM E473 Onset is a point at which the deflection was analyzed first. The peak is a portion having maximum dependent parameter deflection. The peak value is a value corresponding to a maximum deflection from the baseline. 10%, 20%, and 30% show replacement of fine CSA in CSA cement pastes. From the TGA data, as total weight losses are analyzed and thus a linear regression model was developed having a correlation between

Table 6
Results from TGA graphs.

	Peak value (mg)	Peak (°C)	Onset (°C)	Total mass loss (%)
OPC	21.1	53.31	52.7	20.27
CSA	20.65	53.31	52.69	30.4
Fine CSA	20.79	53.35	52.76	32.23
CSA 10%	21.08	52.74	52.74	30.62
CSA 20%	21.11	53.35	52.63	31.08
CSA 30%	17.32	52.8	52.8	30.85

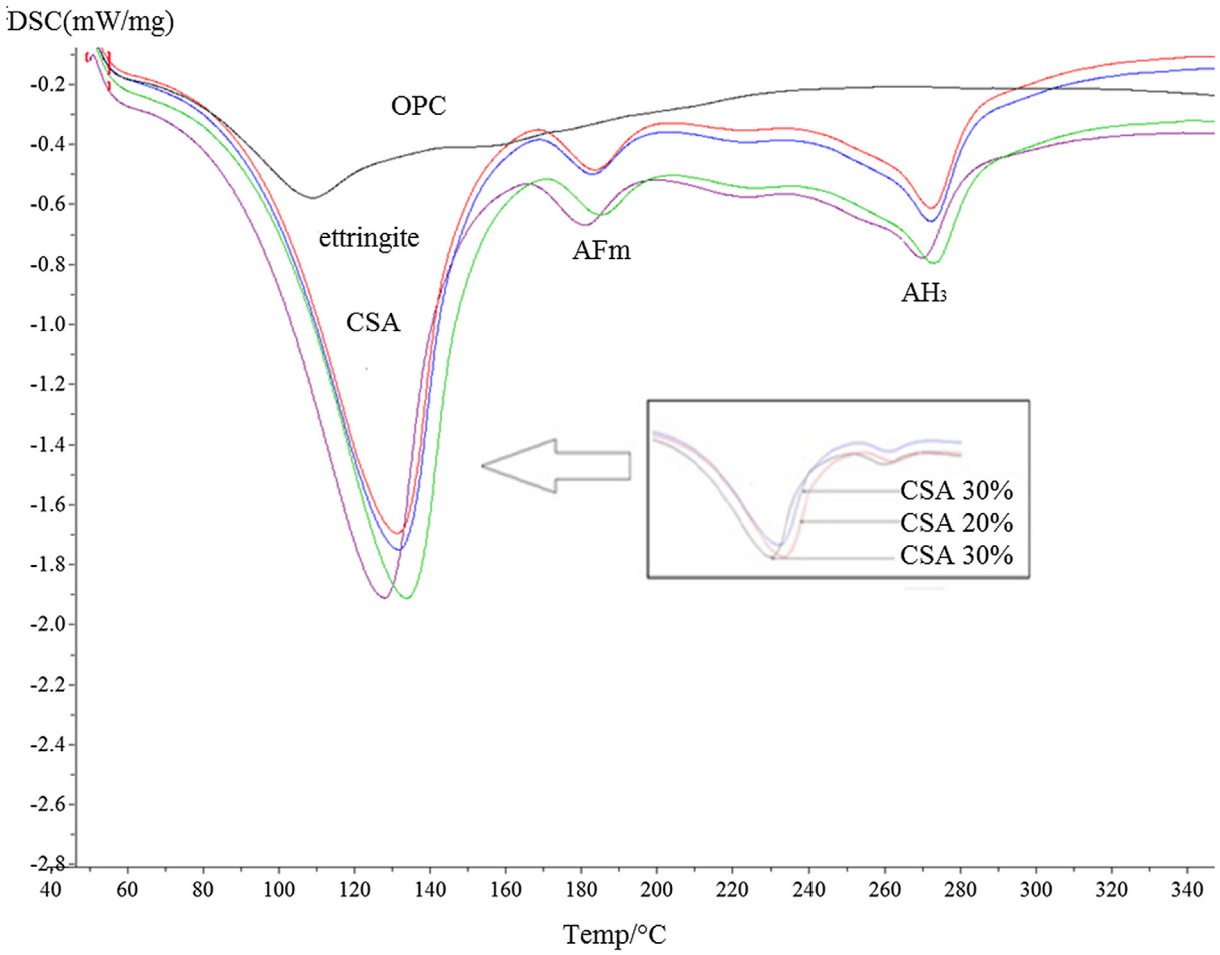

Fig. 9. DTG Curves.

total weight loss in TGA and partial percentage of fine cement with R^2 = 95.4% showing an excellent modal at a 95% confidence interval [50]. Which is shown in Equation (11)

$$TWL = 30.47 + 0.01760b \quad (10)$$

where

TWL = Total weight loss during the thermo gravimetric analysis
b = Replacement of fine CSA in %

According to ASTM C1872 we can calculate the mass percentages of a particular component in the OPC sample as portlandite drops from 350 to 550 °C, calcite drops from 700 to 800 °C while ettringite drops from 100 to 150 °C while other monosulfate temperature drops at 180–200 °C, hemi carbonate temperature drops at 250–280 °C, hydro garnet which drops at 290–310 °C might be overlapping or cannot be developed at this stage because OPC needs more time for development of their hydration products as compared to CSA. The mass percentages with hydration products can be clearly seen in the DTG and TGA curve in Fig. 10.

For CSA samples the possible dehydration phase may include: ettringite (100–150 °C), AFm monosulfate (60–200 °C), strätlingite (130–240 °C), CH Calcium hydroxide (410–510 °C), gypsum (150 °C), C-S-H gel (50–300 °C), and AH_3 (250–280 °C) [51,52]. It can be noted from Fig. 9 fine CSA cement can helps to increase the strength with more ettringite formation as discussed in Section 1. As we cannot calculate their compositions form TGA curve due to the overlapping of peaks but we can calculate the AH_3 content in it as it is an amorphous product in CSA hydrated samples. AH_3 is amorphous below 40 °C and after this, it becomes gibbsite over this temperature [53]. Gibbsite has 3 mol of water and assuming water content to be constant we can calculate the AH_3 content by using an Eq. (12).

$$W_{AH_3} = M_{AH_3} \times W_{H_2O}/3M_{H_2O} \quad (11)$$

where,

W_{AH3} = Weight content of AH_3
W_{H2O} = Weight content of H_2O
M_{AH3} = Molar mass of AH_3
M_{H2O} = Molar mass of H_2O

The AH_3 contents are 14.93, 15.5, 19.04, 15.9, 15.77% for 0, 10%, 20%, 30%, and 100% fine CSA cement replacement respectively. The quadratic relation has been derived between them having R^2 = 88% as shown in Eq. (13). Where W_{AH3} and *b* as defined above. By focusing at Fig. 9 we can see more ettringite content by 20% fine cement replacement.

$$W_{AH3} = 14.93 + 0.04253b - 0.000339b^2 \quad (12)$$

3.5. MIP analysis

Mortar samples are analyzed by Auto Pore IV 9500 V1.09. Table 7 shows different concluding remarks from different samples after 28 days of curing.

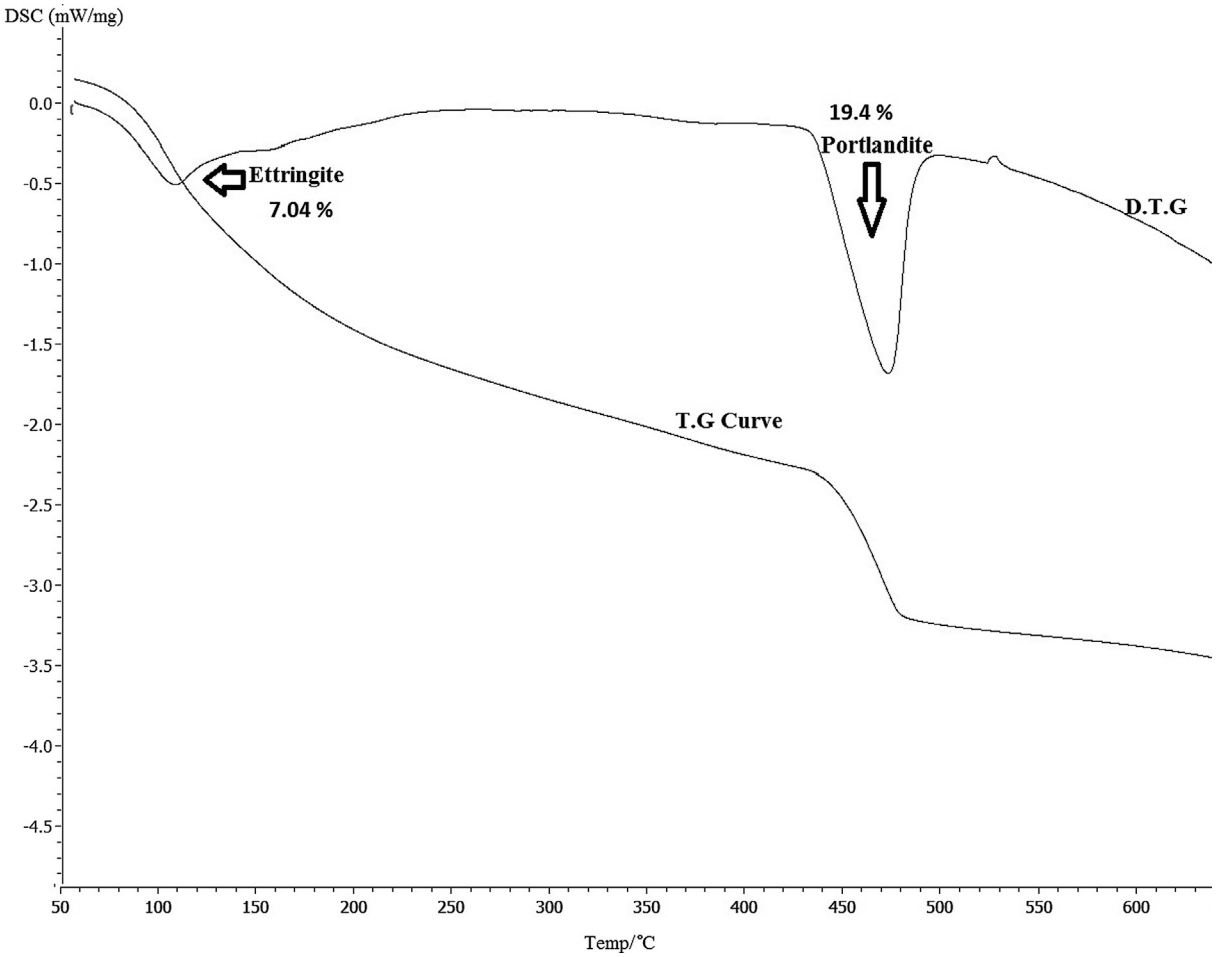

Fig. 10. TGA Analysis of OPC at w/c 0.5.

Table 7
Concluding remarks from MIP.

	OPC	CSA	CSA 10%	CSA 20%	CSA 30%
Total Intrusion Volume (mL/g)	0.16	0.043	0.032	0.023	0.102
Total Pore Area	22.4	6.270	4.879	3.177	12.43
Median Pore Diameter (Area) (nm)	10.4	10.2	9.4	8.7	11.6
Average Pore Diameter (nm)	30.0	27.9	26.6	26.1	28.0
Bulk Density at 0.51 psia (g/mL)	2.30	2.171	2.15	2.19	2.19
Porosity %	16.5	9.49	7.00	5.05	10.56
Permeability (mdarcy)	0.77	0.253	0.25	0.25	0.77
Tortuosity factor	2.10	0.002	0.001	0.00	2.15
Percolation Fractal dimension	2.747	2.845	2.860	2.927	2.748
Backbone Fractal dimension	2.324	2.882	2.884	2.930	2.785

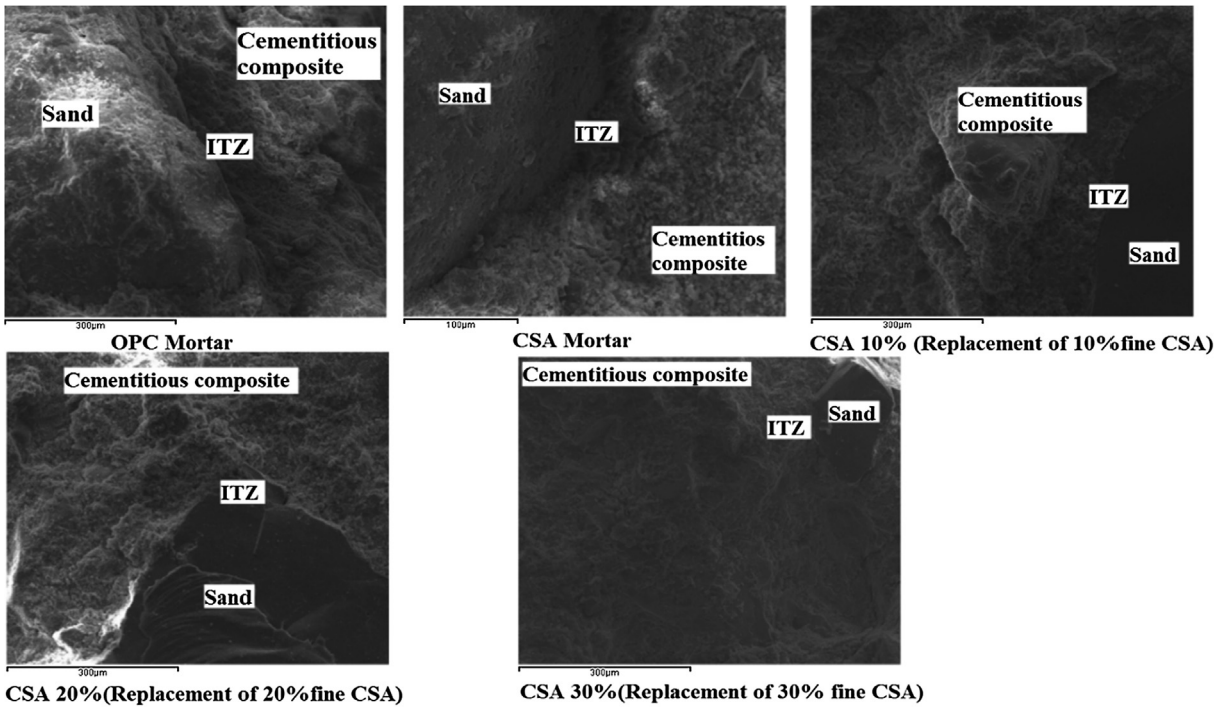

Fig. 11. ITZ locations in SEM pictures.

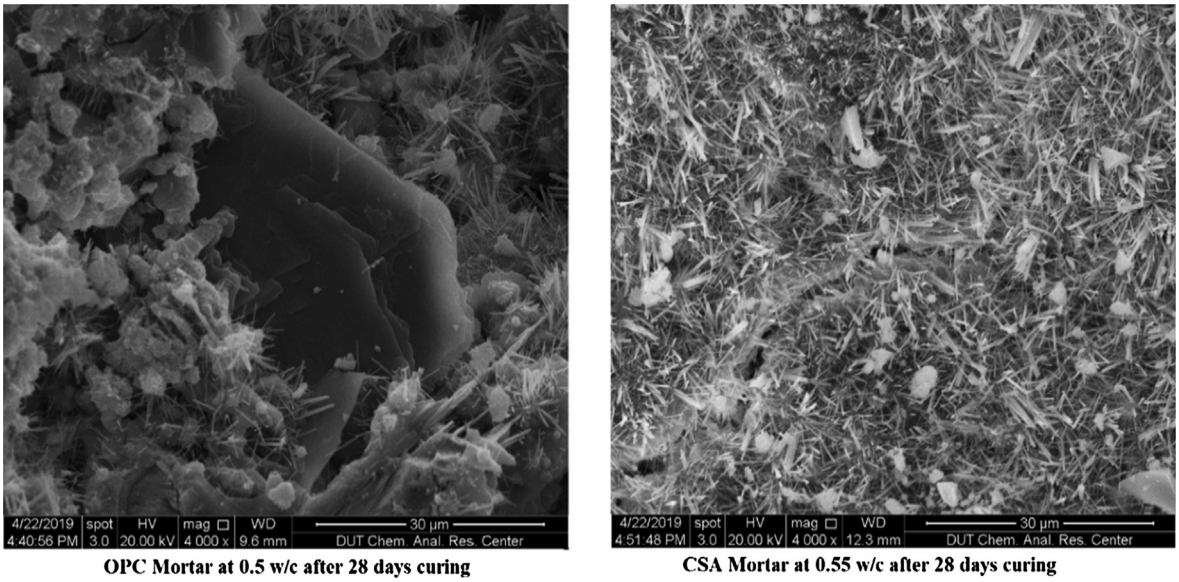

Fig. 12. SEM Pictures of OPC and CSA at high magnifications.

Total intrusion volume is the total volume intruded. The results for intruded volume shows that it is inversely related to particle size as it gives less value as the replacement percentage increases. While total pore values conclude that replacement at 20% fine cement shows less total pores. Median pore diameter concludes that replacement at 20% ground cement shows less median pore diameter which is the main characteristic of pore size. Porosity is a property of voids. More porosity exhibits more voids in the sample. In our case, 20% replacement of fine cement in CSA results in low porosity than others exhibiting fewer voids than other samples. Permeability is a dynamic property and it's related to fluid flow. 20% replacement sample shows less permeability behavior than others. Tortuosity factor is another important parameter which is related to twist and turns of factor. This factor has been neglected in research for many years. Some past research [54,55] shown some interest and importance of tortuosity factor as the relation with permeability. As the permeability is not a straight path in any sample and thus it depends upon the twist and turns of the sample. Since the tortuosity factor in our case for 20% replacement shows null tortuosity factor concluding an excellent model for permeability. Fractal dimension shows a geometric behavior and mechanical properties of the material [56]. In our case, we use two fractal dimensions as one related to percolation while the second is the backbone. The both in our case is high for 20% CSA replacement concludes to show good mechanical properties.

3.6. SEM analysis

By analysis of SEM, We analyzed the position of the interfacial transition zone (ITZ) as shown in Fig. 11. ITZ is also be assumed as a portion having large pores thus showing more porosity structure in the cementitious composite [19]. ITZ thickness is assumed to be less than 50 μm [57].

The content of ettringite is considered to be present in ITZ in CSA systems. By zooming SEM at 40002× magnification focusing at ITZ region showing needle-like crystals which are ettringite. The higher number of ettringite can be observed in the CSA system in Fig. 12 which is also compliance by the results of TGA.

While doing sample preparation for SEM the cutting of the samples leads to small cracks in samples. ITZ is assumed to be the weakest zone. Therefore, the maximum crack occurs in ITZ. The

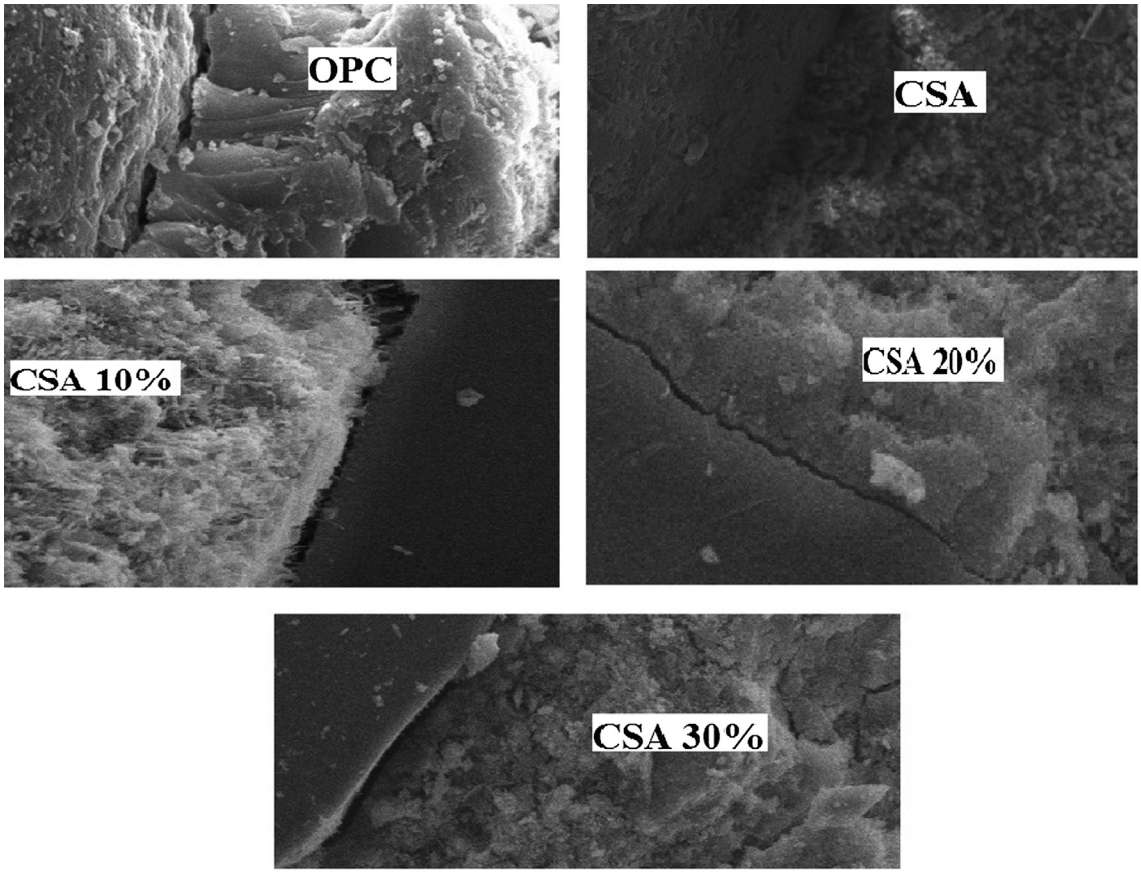

Fig. 13. Cracks in ITZ region.

Table 8
Crack width (um) in ITZ.

	1	2	3	4	5	Average	S.D	Min	Max
OPC	5.66	5.29	3.83	4.19	6.64	5.12	1.139	3.83	6.65
CSA	1.83	2.67	2.32	2.09	3.61	2.50	0.691	1.83	3.61
CSA 10%	1.29	1.29	1.44	2.96	1.49	1.69	0.713	1.29	2.96
CSA 20%	1.46	1.30	1.08	1.64	2.32	1.56	0.472	1.08	2.32
CSA 30%	1.36	1.93	2.65	1.45	2.22	1.92	0.54	1.36	2.65

crack widths which are present in the ITZ is calculated from different samples by using an image J software [58]. The crack width [59] explains the critical failure region at which the structure permeability and porosity are considered to be high and can reduce structure serviceability [60]. It can be discovered that the sand grain is separated from the cementitious matrix which leads to crack. The crack surface at ITZ is zoomed and is shown in Fig. 13 at 4000× magnification.

The crack width in ITZ at 5 different places in the crack boundary is investigated. The results are shown in Table 8. It must be emphasized that crack widths in 20% replacement of fine CSA result in less crack width. CSA cement also shows good crack width behavior as compared to OPC due to excellent microstructure. The results from crack width conclude that the effect of fine cement replacement at 20% can help to reduce crack widths in cementitious composites. Grey level graphs in image J software shows different peaks. It makes the graph between the heights of phases with relative fractions which also depends upon the effect of the widening of the peaks. In our samples, pores can be easily recognized with the help of grey value analysis as shown in Fig. 14 as compared to other hydration products because pores peak doesn't overlap in that analysis.

From grey value, we can only analyze the pore location but cannot identify the pore size clearly due to the very dense structure. As CSA is finer than OPC cement and the ITZ depends upon the size of the cement particles as discussed in Fig. 1.

3.7. Image J analysis

Image J analysis helps us to find porosity of different samples [61]. By using appropriate threshold values in image J analysis software we can able to analyze particles. Fig. 15 shows different binary images at different angles and surfaces of samples imported from SEM images. And then it helps to find the porosity.

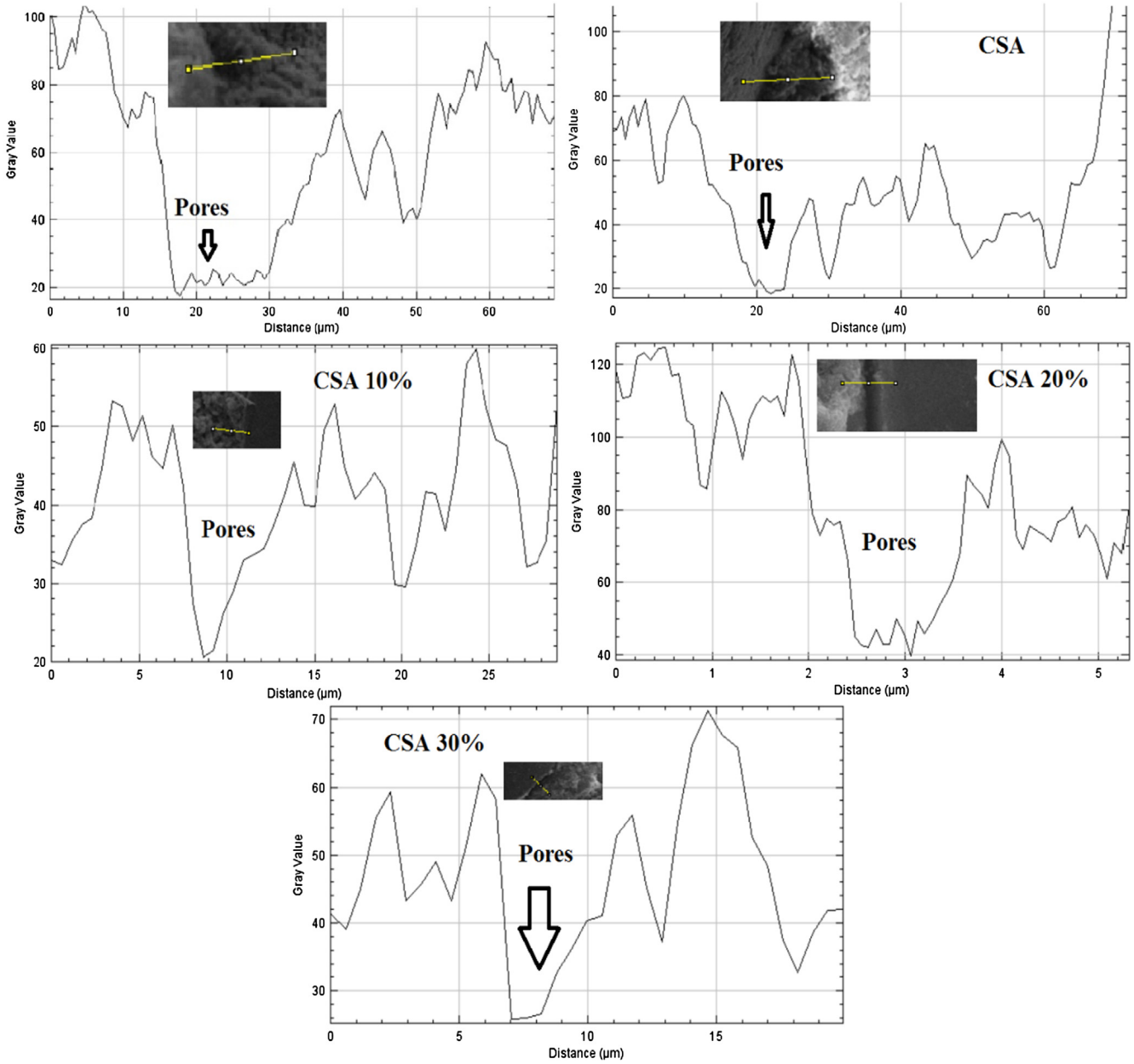

Fig. 14. Pores analysis using grey value.

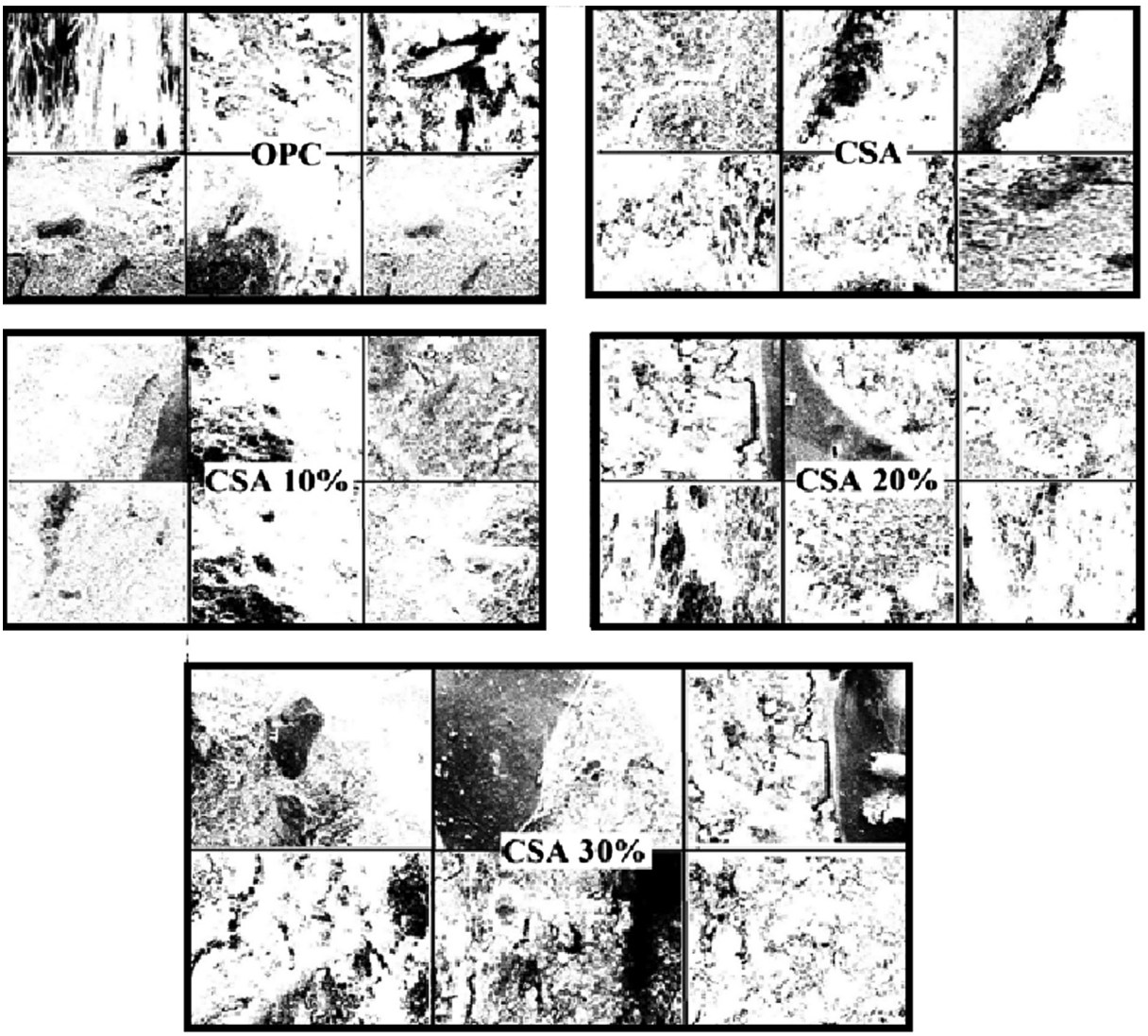

Fig. 15. Binary images at different angles & surfaces of samples.

Table 9
Average analyze particles by Image J.

Slice	Average Count	Mean Total Area	Average %Area
OPC	4344	4243.54	27.98
CSA	2246.16	4782.78	16.39
CSA 10%	6367.5	13720.44	15.49
CSA 20%	783.33	4393.22	10.47
CSA 30%	196.33	89682.19	16.52

Different porosity results after no of iterations have been shown in Table 9. Where the average % area defined as a pore area in samples. The results show that a 20% replacement in CSA mortar concludes good porosity results. And the results from Image J software are also compliance with MIP.

4. Discussion

The replacement of 20% fine cement in conventional CSA cement reveals in higher flexural and compressive strength as well as energy absorption capacities. More than 20% replacement of fine cement shows less flexural and compressive strength. This might be due to agglomeration and distribution of fine particles in the matrix of cementitious composites. Also, too many fine particles cannot take part in strength development and attain different hydration heats. The more needle-like content ettringite and AH_3 contributes to more strength development at early stages as verified by TGA results of 20% replacement of fine CSA. ITZ has many important roles in the properties of mortar and concrete. It is generally assumed that higher porosity region in a structure contributes to ITZ [5]. From Fig. 1 it can be concluded that there could be some optimum size for cement particles which can control the ITZ thickness and can resist structure from vulnerable attacks. The 20% replacement results in less pore structure which might be due to the filling effect of cement sand paste while mixing of mortar preparation and results in less ITZ thickness. The hydration products in replacement of fine CSA results in fewer microspores and dense structure [4]. Filling effect covers the cement particles from fine sand paste results in the effective microstructure. The reason behind this phenomenon is basically the fine particles help to fill the spaces resulting to fill the wall effect in ITZ. Therefore, this research concludes that CSA replacement of 20% fine cement by fine cement sand paste mortar preparation technique exhibits effective microstructure.

5. Conclusions

In this research, the influence of fine cement sand paste in mortar preparation is studied with a wide range of experimental techniques. For the preparation of fine cement mortar, a new method is applied which have the following advantages.

(1) For mortar preparation of fine cement, the fine cement and sand particles are mixed and then conventional cement is added to form mortar. Therefore, the cement particles are covered by fine cement particles resulting in fewer pores. Thus, ultimately have excellent microstructure characteristics.
(2) The amount of fine CSA having an average diameter of 2.4 μm placed with an optimum dosage of 20% in conventional CSA system resulted in improved overall strength by 30–35%. The porosity and permeability were reduced by 60–70% which was discovered by MIP and image J analysis. In addition, the crack widths in ITZ were also reduced up to 60% as compared to OPC system.
(3) At the early stage of hydration, the 20% replacement of fine CSA an average diameter of 2.4 μm in conventional CSA cement has attained more ettringite and AH_3 content. Thus contributes towards more rapid strength development than OPC system.
(4) The new technique for mixing fine cement for mortar preparation is found to be beneficial and can be used for future reference in cement and concrete batching plants.

Declaration of Competing Interest

The authors declare that they have no known competing financial interests or personal relationships that could have appeared to influence the work reported in this paper.

Acknowledgments

This work is supported by the international collaboration and exchange program from the NSFC-RCUK/EPSRC with grant No. 51761135011 and National Natural Science Foundation of China with grant No 51472041. The financial support from China Scholarship Council (CSC) for PhD studies of first author at Dalian University of Technology, China is gratefully acknowledged. The authors are also thankful to Jiye Li and Engr. Mehran Khan for their help during the research work. The careful review and constructive suggestions by the anonymous reviewers are gratefully acknowledged.

References

[1] I.B. Celik, The effects of particle size distribution and surface area upon cement strength development, Powder Technol. 188 (2009) 272–276, https://doi.org/10.1016/j.powtec.2008.05.007.
[2] M.S. Amin, S.M.A. El-Gamal, S.A. Abo-El-Enein, F.I. El-Hosiny, M. Ramadan, Physico-chemical characteristics of blended cement pastes containing electric arc furnace slag with and without silica fume, HBRC J. 11 (2015) 321–327, https://doi.org/10.1016/j.hbrcj.2014.07.002.
[3] S.A. Abo-El-Enein, F.S. Hashem, M.S. Amin, D.M. Sayed, Physicochemical characteristics of cementitious building materials derived from industrial solid wastes, Constr. Build. Mater. 126 (2016) 983–990, https://doi.org/10.1016/j.conbuildmat.2016.09.112.
[4] S.M.A. El-Gamal, F.I. El-Hosiny, M.S. Amin, D.G. Sayed, Ceramic waste as an efficient material for enhancing the fire resistance and mechanical properties of hardened Portland cement pastes, Constr. Build. Mater. 154 (2017) 1062–1078, https://doi.org/10.1016/j.conbuildmat.2017.08.040.
[5] B. Zhang, H. Tan, B. Ma, F. Chen, Z. Lv, X. Li, Preparation and application of fine-grinded cement in cement-based material, Constr. Build. Mater. 157 (2017) 34–41, https://doi.org/10.1016/j.conbuildmat.2017.09.023.
[6] M.S. Konsta-Gdoutos, Z.S. Metaxa, S.P. Shah, Multi-scale mechanical and fracture characteristics and early-age strain capacity of high performance carbon nanotube/cement nanocomposites, Cem. Concr. Compos. 32 (2010) 110–115, https://doi.org/10.1016/j.cemconcomp.2009.10.007.
[7] R. Chandran, M. Gifty, A. Honeyta, Simplified equation for young's modulus of CNT reinforced concrete, AIP Adv. 7 (2017) 125122, https://doi.org/10.1063/1.5011319.
[8] W. Li, S. Kawashima, J. Xiao, D.J. Corr, C. Shi, S.P. Shah, Comparative investigation on nanomechanical properties of hardened cement paste, Mater. Struct. 49 (2016) 1591–1604, https://doi.org/10.1617/s11527-015-0597-3.
[9] S.L. Sarkar, J. Wheeler, Microstructural development in an ultrafine cement—Part II, Cem. Concr. Res. 31 (2001) 125–128, https://doi.org/10.1016/S0008-8846(00)00394-X.
[10] N.A. Toprak, A.H. Benzer, Effects of grinding aids on model parameters of a cement ball mill and an air classifier, Powder Technol. 344 (2019) 706–718, https://doi.org/10.1016/j.powtec.2018.12.039.
[11] H.O. Njoku, O.R. Bafuwa, C.A. Mgbemene, O.V. Ekechukwu, Benchmarking energy utilization in cement manufacturing processes in Nigeria and estimation of savings opportunities, Clean Technol. Environ. Policy 19 (2017) 1639–1653, https://doi.org/10.1007/s10098-017-1353-x.
[12] J.H. Sharp, C.D. Lawrence, R. Yang, Calcium sulfoaluminate cements—low-energy cements, special cements or what?, Adv Cem. Res. 11 (1999) 3–13, https://doi.org/10.1680/adcr.1999.11.1.3.
[13] J. Zhao, G. Cai, D. Gao, S. Zhao, Influences of freeze-thaw cycle and curing time on chloride ion penetration resistance of sulphoaluminate cement concrete, Constr. Build. Mater. 53 (2014) 305–311, https://doi.org/10.1016/j.conbuildmat.2013.11.110.
[14] P.K. Mehta, Investigations on Energy Saving Cements, World Cem. Technology, 1980. https://www.worldcement.com.
[15] G. Bernardo, A. Telesca, G.L. Valenti, A porosimetric study of calcium sulfoaluminate cement pastes cured at early ages, Cem. Concr. Res. 36 (2006) 1042–1047, https://doi.org/10.1016/j.cemconres.2006.02.014.
[16] H. Tan, X. Zhang, X. He, Y. Guo, X. Deng, Y. Su, J. Yang, Y. Wang, Utilization of lithium slag by wet-grinding process to improve the early strength of sulphoaluminate cement paste, J. Clean. Prod. 205 (2018) 536–551, https://doi.org/10.1016/j.jclepro.2018.09.027.
[17] F. Kontoleontos, P.E. Tsakiridis, A. Marinos, V. Kaloidas, M. Katsioti, Influence of colloidal nanosilica on ultrafine cement hydration: Physicochemical and microstructural characterization, Constr. Build. Mater. 35 (2012) 347–360, https://doi.org/10.1016/j.conbuildmat.2012.04.022.
[18] J. Zhang, X. Guan, H. Li, X. Liu, Performance and hydration study of ultra-fine sulfoaluminate cement-based double liquid grouting material, Constr. Build. Mater. 132 (2017) 262–270, https://doi.org/10.1016/j.conbuildmat.2016.11.135.
[19] K.L. Scrivener, A.K. Crumbie, P. Laugesen, The Interfacial Transition Zone (ITZ) between cement paste and aggregate in concrete, Interface Sci. 12 (2004) 411–421, https://doi.org/10.1023/b:ints.0000042339.92990.4c.
[20] S.H. Kosmatka, B. Kerkhoff, W.C. Panarese, N.F. MacLeod, R.J. McGrath, Designing and Proportioning Normal Concrete Mixtures, 14th ed., Portland cement association, 2002. www.cement.org.
[21] E.J. Garboczi, D.P. Bentz, Analytical formulas for interfacial transition zone properties, Adv. Cem. Based Mater. 6 (1997) 99–108, https://doi.org/10.1016/S1065-7355(97)90016-X.
[22] J. Jiang, G. Sun, C. Wang, Numerical calculation on the porosity distribution and diffusion coefficient of interfacial transition zone in cement-based composite materials, Constr. Build. Mater. 39 (2013) 134–138, https://doi.org/10.1016/j.conbuildmat.2012.05.023.
[23] P.K. Mehta, Concrete Structure, Properties and Materials, first ed., Prentice-Hall, 1986.
[24] K.-Y. Liao, P.-K. Chang, Y.-N. Peng, C.-C. Yang, A study on characteristics of interfacial transition zone in concrete, Cem. Concr. Res. 34 (2004) 977–989, https://doi.org/10.1016/j.cemconres.2003.11.019.
[25] H.S. Wong, N.R. Buenfeld, Patch microstructure in cement-based materials: fact or artefact?, Cem Concr. Res. 36 (2006) 990–997, https://doi.org/10.1016/j.cemconres.2006.02.008.
[26] J. Tragardh, Microstructural features and related properties of self-compacting concrete, in: First Int. RILEM Symp. Self-Compacting Concr., 1999, pp. 175–186.
[27] Y. Gao, X. Zhu, D.J. Corr, M.S. Konsta-Gdoutos, S.P. Shah, Characterization of the interfacial transition zone of CNF-Reinforced cementitious composites, Cem. Concr. Compos. 99 (2019) 130–139, https://doi.org/10.1016/j.cemconcomp.2019.03.002.
[28] P. Carrara, L. De Lorenzis, Consistent identification of the interfacial transition zone in simulated cement microstructures, Cem. Concr. Compos. 80 (2017) 224–234, https://doi.org/10.1016/j.cemconcomp.2017.03.008.
[29] D.P. Bentz, Blending different fineness cements to engineer the properties of cement-based materials, Mag. Concr. Res. 62 (2010) 327–338, https://doi.org/10.1680/macr.2008.62.5.327.
[30] W. Shen, Y. Liu, B. Yan, J. Wang, P. He, C. Zhou, X. Huo, Cement industry of China: driving force, environment impact and sustainable development, Renew. Sustain. Energy Rev. 75 (2017) 618–628, https://doi.org/10.1016/j.rser.2016.11.033.
[31] ASTM D6913-04R2009, Standard Test Methods for Particle-size Distribution (gradation) of Soils Using Sieve Analysis, ASTM Int., West Conshohocken, PA, 2004, pp. 1–35. doi:10.1520/D6913-04R09.2.

[32] ASTM-E2651, Standard guide for powder particle size analysis, ASTM Int. (2010) 1–8, https://doi.org/10.1520/E2651-10.
[33] ASTM-C1437, Test method for slump of hydraulic cement concrete, (2005) 12–15. doi:10.1520/C1437-15.2.
[34] T. Saito, Y. Fujikura, I. Ide, S. Date, Effect of rheological property on fluidity of fresh mortar under vibration, J. Eng. Appl. Sci. 12 (2017) 2720–2724.
[35] T. Saito, Y. Fujikura, S. Hashimoto, S. Date, Study on the rheological properties of fresh mortar under vibration, Int. J. Struct. Civ. Eng. Res. (2015), https://doi.org/10.18178/ijscer.4.3.291-295.
[36] ASTM-C348, Flexural strength of hydraulic-cement mortars, ASTM Int. (1998) 2–7, https://doi.org/10.1520/C0348-14.2.
[37] ASTM-C349, Standard test method for compressive strength of hydraulic-cement mortars (using portions of prisms broken in flexure), ASTM Int. (1997) 1–4, https://doi.org/10.1520/C0349-97.
[38] ASTM C-1702, Standard test method for measurement of heat of hydration of hydraulic cementitious materials using isothermal conduction calorimetry, Annu. B. ASTM Stand. 9 (2017), https://doi.org/10.1520/C1702-17.
[39] ASTM E1142-15, Standard terminology relating to thermophysical properties, ASTM E1142-15. (2015) 1–8. doi:10.1520/E1142-15.2.
[40] ASTM D4404-10, Standard Test method for determination of pore volume and pore volume distribution of soil and rock by mercury intrusion porosimetry, Astm Int. (2014) 1–7, https://doi.org/10.1520/D4404-10.
[41] S. Diamond, The microstructure of cement paste and concrete – a visual primer, Cem. Concr. Compos. 26 (2004) 919–933, https://doi.org/10.1016/j.cemconcomp.2004.02.028.
[42] K.C. Torres, K.C. Torres, Specimen preparation for scanning electron microscopy, in: Tissue Cult. Tech. Hortic. Crop., 1989, pp. 225–233. doi:10.1007/978-1-4615-9756-8_28.
[43] P.E. Stutzman, Scanning electron microscopy in concrete petrography, in: Mater. Sci. Concr. Spec. Vol. Hydroxide Concr., 2000, pp. 59–72.
[44] P. Bühler, P. Schlaich, Image J (2013) 237–253, https://doi.org/10.1007/978-3-642-37942-0_12.
[45] C. Grove, D.A. Jerram, jPOR: an image J macro to quantify total optical porosity from blue-stained thin sections, Comput. Geosci. 37 (2011) 1850–1859, https://doi.org/10.1016/J.CAGEO.2011.03.002.
[46] F. Winnefeld, B. Lothenbach, Hydration of calcium sulfoaluminate cements – experimental findings and thermodynamic modelling, Cem. Concr. Res. 40 (2010) 1239–1247, https://doi.org/10.1016/j.cemconres.2009.08.014.
[47] R.E. Miller, Multiple Regression (1986), https://doi.org/10.1007/978-1-4614-5743-5_4.
[48] W.S. Ansari, Z. ur Rehman, M.J. Thaheem, U. Khalid, A statistical review of offsite construction techniques in Pakistan, Sci. Int. 27 (2015) 5069–5074.
[49] M. Khan, M. Cao, M. Ali, Effect of basalt fibers on mechanical properties of calcium carbonate whisker-steel fiber reinforced concrete, Constr. Build. Mater. 192 (2018) 742–753, https://doi.org/10.1016/j.conbuildmat.2018.10.159.
[50] W.S. Ansari, M.J. Thaheem, M.M.A. Khalfan, Use of offsite construction techniques in Pakistan, Middle East J. Manag. 3 (2016) 218, https://doi.org/10.1504/mejm.2016.10000653.
[51] J. Li, J. Chang, Effect of crystal/amorphous ratio on mechanical properties in a C 4 A 3 $-C 2 S hydration system with or without gypsum addition, Constr. Build. Mater. 208 (2019) 36–45, https://doi.org/10.1016/j.conbuildmat.2019.03.004.
[52] D. Wang, J. Chang, W.S. Ansari, The effects of carbonation and hydration on the mineralogy and microstructure of basic oxygen furnace slag products, J. CO2 Util. 34 (2019) 87–98, https://doi.org/10.1016/j.jcou.2019.06.001.
[53] J. Chang, Y. Zhang, X. Shang, J. Zhao, X. Yu, Effects of amorphous AH_3 phase on mechanical properties and hydration process of C_4A_3S-CSH_2-CH-H_2O system, Constr. Build. Mater. 133 (2017) 314–322, https://doi.org/10.1016/j.conbuildmat.2016.11.111.
[54] A. Atkinson, A.K. Nickerson, The diffusion of ions through water-saturated cement, J. Mater. Sci. 19 (1984) 3068–3078, https://doi.org/10.1007/bf01026986.
[55] E.J. Garboczi, Permeability, diffusivity, and microstructural parameters: a critical review, Cem. Concr. Res. 20 (1990) 591–601, https://doi.org/10.1016/0008-8846(90)90101-3.
[56] X. Yang, F. Wang, X. Yang, Q. Zhou, Fractal dimension in concrete and implementation for meso-simulation, Constr. Build. Mater. (2017) 464–472, https://doi.org/10.1016/j.conbuildmat.2017.03.157.
[57] G. Sun, W. Sun, Y. Zhang, Z. Liu, Quantitative analysis and affecting factors of the overlapping degree of interfacial transition zone between neighboring aggregates in concrete, J. Wuhan Univ. Technol. Mater. Sci. Ed. 26 (2011) 147–153, https://doi.org/10.1007/s11595-011-0187-3.
[58] E. Adili, M.R. Sohrabi, Effect of Nano-Sio2 on Crack Width in ITZ (SEM Observation), 2 (2012) 3386–3390.
[59] X.F. Wang, Y.J. Huang, G.Y. Wu, C. Fang, D.W. Li, N.X. Han, F. Xing, Effect of nano-Sio2 on strength, shrinkage and cracking sensitivity of lightweight aggregate concrete, Constr. Build. Mater. 175 (2018) 115–125, https://doi.org/10.1016/j.conbuildmat.2018.04.113.
[60] G.L. Golewski, Evaluation of morphology and size of cracks of the Interfacial Transition Zone (ITZ) in concrete containing fly ash (FA), J. Hazard. Mater. 357 (2018) 298–304, https://doi.org/10.1016/j.jhazmat.2018.06.016.
[61] W.S. Ansari, Porosity analysis using Image J, 8th Grad. Forum Build. Mater., Southeast University, Nanjing, China, 2019.